

Dark-state-based three-element vector model for the stimulated Raman interaction

M. S. Shahriar,¹ P. R. Hemmer,² D. P. Katz,³ A. Lee,³ and M. G. Prentiss³

¹Research Laboratory of Electronics, Massachusetts Institute of Technology, Cambridge, Massachusetts 02139

²Rome Laboratory, Hanscom Air Force Base, Massachusetts 01731

³Department of Physics, Harvard University, Cambridge, Massachusetts 02138

(Received 18 December 1995; revised manuscript received 30 July 1996)

In this paper we develop a three-element vector model to describe the stimulated Raman interaction in a Λ system. This model is valid over the range of interaction energies for which the excited state follows the ground states adiabatically. We use the model to present simple physical interpretations of the generation of Raman-Ramsey fringes in a separated field excitation, the ac Stark shift in the Raman clock, the ultrahigh-resolution mapping of microwave phase using Raman probes, and the coherent transfer of population by adiabatic passage for atomic beam splitters. The expressions for observables are derived by inspection and agree quantitatively with published experimental results. [S1050-2947(97)00302-8]

PACS number(s): 42.65.Dr, 32.80.Wr

I. INTRODUCTION

Recently, there has been much interest in potential applications of the Raman interaction in a Λ -type three-level system, where the upper state is short lived and the low-lying states are long lived. The applications include the Raman clock [1–3], frequency conversion using Raman lasing [4,5], Raman phase conjugation [6,7], generation of squeezed states [8], lasing without inversion [9], optical mapping of microwave phase and optical deflection of millimeter waves [10], Raman-induced spin echo for optical data storage and image processing [11], ultrahigh resolution position sensing [12], atomic interferometry [13–15], atomic beam deflection [16], and subrecoil cooling of atoms [17–19]. For these and potentially other applications, it is useful to understand the time-dependent behavior of the Raman interaction.

For a closed system, the optical Bloch equations for the Λ system involve eight real variables. Numerical methods have been employed to determine the time evolution of the system, but this approach does not greatly enhance one's intuition. As an alternative, several authors [20] have used the dressed states to illustrate the fundamental features such as population trapping in the Raman interaction. The dressed-state basis was extended to develop a coupled-pendulum model [21] for further insight. Variations of this model have also been used to illustrate the behavior of optical forces on a Λ -system atom [22]. However, this model does not take into account the influx of spontaneously decaying atoms into the two low-lying states, so that the results obtained are only qualitatively correct. When the source terms are included [19], the dressed states optical Bloch equations are no longer easy to interpret.

In this paper, we develop a model to describe the Λ system under stimulated Raman excitation that is easy to interpret physically, but at the same time can be used to find analytical solutions for the time-dependent behavior of observables, often by mere inspection. This model is valid over the range of interaction energies for which the excited state follows the two ground states adiabatically. In this limit (consistent with many cases of experimental interest), the Raman interaction is represented by the ground-state dynamics, thus reducing the optical Bloch equations to three real

variables. The time evolution of these three variables (and thus the entire system) is modeled by the motion of a three-element vector. The ground-state population difference and coherence are directly manifested by this vector. In addition, we show how other observables, such as the excited-state population and its coherences with the ground states, can also be read directly off this vector.

This model has two main features: it provides a clear physical interpretation of the transient behavior of the system and it is designed to handle the cases of unequal and/or time-varying Rabi frequencies simply. The motion of the vector can be interpreted physically in terms of partially diagonalized states so that one can find explicit expressions for the time-dependent observables by simply drawing a diagram. For example, we show how the expression for the ac Stark shift of the Raman-Ramsey fringes can be found without solving any equations at all. We also show how this model can be used to compute observables in microwave phase-sensitive optical absorption. The results obtained in this way are seen to agree well with experimental data reported earlier [3,10]. The model also describes low-intensity adiabatic passage in a bichromatic standing wave in a simple and physically illuminating manner.

II. THE STIMULATED RAMAN INTERACTION

A. Basic theory

Figure 1 illustrates schematically the Λ system under stimulated Raman excitation. Here the excited state $|e\rangle$ is short lived and the two low-lying ground states $|a\rangle$ and $|b\rangle$ are long lived. The light at frequency ω_1 couples $|a\rangle$ to $|e\rangle$, while the light at ω_2 couples $|b\rangle$ to $|e\rangle$ as shown. Both couplings are electric-dipole interactions, whose strengths are given by the Rabi frequencies

$$g_1 \equiv \frac{\boldsymbol{\mu}_{ae} \cdot \mathbf{E}_1}{\hbar}, \quad g_2 \equiv \frac{\boldsymbol{\mu}_{be} \cdot \mathbf{E}_2}{\hbar}, \quad (1)$$

where $\boldsymbol{\mu}$ is the dipole moment operator of the atom. The laser detunings $\delta_1 \equiv \omega_1 - (\epsilon_e - \epsilon_a)/\hbar$ and $\delta_2 \equiv \omega_2 - (\epsilon_e - \epsilon_b)/\hbar$ are used to define the difference detuning as $\Delta \equiv \delta_1 - \delta_2$ and the common mode detuning as $\delta \equiv \frac{1}{2}(\delta_1 + \delta_2)$. Finally, the in-

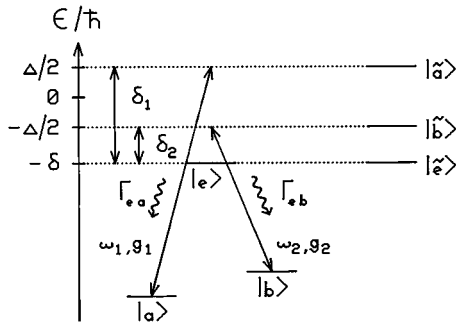


FIG. 1. Energy diagram of the Λ system under stimulated Raman excitation. Shown are the coupling strengths and frequencies, detunings, and decay rates. The states $|a\rangle$, $|b\rangle$, and $|e\rangle$ represent those of the three-level atom alone. The states $|\tilde{a}\rangle$, $|\tilde{b}\rangle$, and $|\tilde{e}\rangle$ represent the atom-field composite states that form what we refer to as the atomic states basis. The energies are shown at the left, in terms of the difference and common mode detunings.

dividual decay rates are given by Γ_{ea} and Γ_{eb} and the total decay rate is given by Γ . Note that we assume a closed system, so that atoms decaying from the excited state enter one or the other of the ground states.

In this paper we use a semiclassical approach in which the laser field is expressed classically as

$$\mathbf{E}(\mathbf{r}, t) = \frac{1}{2}[\mathbf{E}_1(\mathbf{r})e^{-i\omega_1 t} + \text{c.c.}] + \frac{1}{2}[\mathbf{E}_2(\mathbf{r})e^{-i\omega_2 t} + \text{c.c.}], \quad (2)$$

where \mathbf{r} is the position (c.m.) of the atom and ω_1 and ω_2 are the frequencies of the optical fields. Here we will concentrate on the case where $\mathbf{E}_1(\mathbf{r})$ and $\mathbf{E}_2(\mathbf{r})$ are traveling plane waves, implying that the field amplitudes and Rabi frequencies are independent of position. In the atomic states basis the Hamiltonian for the stimulated Raman interaction in the electric-dipole and rotating-wave approximations is

$$H = \hbar \begin{bmatrix} \epsilon_a/\hbar & 0 & -\frac{1}{2}g_1^*e^{+i\omega_1 t} \\ 0 & \epsilon_b/\hbar & -\frac{1}{2}g_2^*e^{+i\omega_2 t} \\ -\frac{1}{2}g_1e^{-i\omega_1 t} & -\frac{1}{2}g_2e^{-i\omega_2 t} & \epsilon_e/\hbar \end{bmatrix}, \quad (3)$$

where the ϵ_i are the energies of the atomic states, and the basis vectors are

$$|a\rangle = \begin{bmatrix} 1 \\ 0 \\ 0 \end{bmatrix}, \quad |b\rangle = \begin{bmatrix} 0 \\ 1 \\ 0 \end{bmatrix}, \quad |e\rangle = \begin{bmatrix} 0 \\ 0 \\ 1 \end{bmatrix}. \quad (4)$$

It is convenient to transform the Hamiltonian to the rotating-wave basis, which is spanned by the atom-field composite states

$$|\tilde{a}\rangle \equiv |a\rangle|\omega_1\rangle \equiv \begin{bmatrix} 1 \\ 0 \\ 0 \end{bmatrix}, \quad |\tilde{b}\rangle \equiv |b\rangle|\omega_2\rangle \equiv \begin{bmatrix} 0 \\ 1 \\ 0 \end{bmatrix}, \quad (5)$$

$$|\tilde{e}\rangle \equiv |e\rangle \equiv \begin{bmatrix} 0 \\ 0 \\ 1 \end{bmatrix},$$

where $|\omega_1\rangle$ and $|\omega_2\rangle$ are semiclassical photon states. In this basis, which we will call the composite states basis, the Hamiltonian can be written as

$$\tilde{H} = \frac{\hbar}{2} \begin{bmatrix} \Delta & 0 & -g_1^* \\ 0 & -\Delta & -g_2^* \\ -g_1 & -g_2 & -2\delta - i\Gamma \end{bmatrix}, \quad (6)$$

where we have chosen the zero of energy such that $\delta + \epsilon_e/\hbar = 0$. We have also added the damping rate to the Hamiltonian to account for spontaneous decay directly. A diagram of the energy levels of the atom-field composite states is illustrated in Fig. 1. The equation of motion for the density matrix can then be written as

$$\dot{\tilde{\rho}} = \frac{i}{\hbar} [\tilde{\rho}\tilde{H}^\dagger - \tilde{H}\tilde{\rho}] + \tilde{L}\tilde{\rho}\tilde{e}\tilde{e}, \quad (7)$$

where $\tilde{\rho}$ is the rotating-wave density operator represented in the basis of Eq. (5) and \tilde{L} is the source matrix

$$\tilde{L} = \begin{bmatrix} \Gamma_{ea} & 0 & 0 \\ 0 & \Gamma_{eb} & 0 \\ 0 & 0 & 0 \end{bmatrix}. \quad (8)$$

The physical process governing the Raman interaction is more transparent in a basis in which the Raman trapped state is one of the basis vectors. We will use this approach in deriving as well as interpreting the three-element vector model. However, since most of the familiar observables are expressed in the basis of Eq. (5), we will interpret the results in that basis as well.

B. The Raman interaction in terms of the trapped state

The trapped state is a coherent superposition of the two ground states, weighted in such a way that there is no net dipole moment coupling this state to the excited state. We denote the trapped state as $|-\rangle$ and its orthogonal states as $|+\rangle$ and $|e\rangle$, where both $|-\rangle$ and $|+\rangle$ are coherent superpositions of ground states only. The properly normalized expressions for the basis states $|-\rangle$, $|+\rangle$, and $|e\rangle$, are

$$|-\rangle = \cos\theta|\tilde{a}\rangle - \sin\theta|\tilde{b}\rangle,$$

$$|+\rangle = \sin\theta|\tilde{a}\rangle + \cos\theta|\tilde{b}\rangle, \quad |e\rangle = |\tilde{e}\rangle, \quad (9)$$

where $\sin\theta = g_1/g$, $\cos\theta = g_2/g$, and $g = \sqrt{g_1^2 + g_2^2}$. This partially diagonalized basis can be formally expressed by the transformation matrix R :

$$R = \begin{bmatrix} \cos\theta & -\sin\theta & 0 \\ \sin\theta & \cos\theta & 0 \\ 0 & 0 & 1 \end{bmatrix}. \quad (10)$$

The equation of motion for the density matrix in this basis is given by

$$\dot{\rho} = \frac{i}{\hbar} [\rho H^\dagger - H\rho] + L\rho ee, \quad (11)$$

where

$$\rho = R \tilde{\rho} R^{-1}, \quad (12)$$

and similarly for H and L . Note that $\tilde{\rho}_{\bar{e}\bar{e}} = \rho_{ee}$ is a constant under this transformation. The transformed Hamiltonian is

$$H = \frac{\hbar}{2} \begin{bmatrix} C\Delta & S\Delta & 0 \\ S\Delta & -C\Delta & -g \\ 0 & -g & -2\delta - i\Gamma \end{bmatrix}, \quad (13)$$

where $C \equiv \cos 2\theta$ and $S \equiv \sin 2\theta$, and the transformed source matrix is

$$L = \frac{\Gamma}{2} \begin{bmatrix} 1 + Cd & Sd & 0 \\ Sd & 1 - Cd & 0 \\ 0 & 0 & 0 \end{bmatrix}, \quad (14)$$

where $d \equiv (\Gamma_{ea} - \Gamma_{eb})/\Gamma$ is the normalized difference between the rates of decay to states $|a\rangle$ and $|b\rangle$.

To interpret the Raman interaction in this basis, consider first the elements of the Hamiltonian. $H_{--} = \hbar C\Delta/2$ ($H_{++} = -\hbar C\Delta/2$) represents the energy of the $|-\rangle$ ($|+\rangle$) state and can be seen simply as the weighted sum of the energies of the constituent states $|\bar{a}\rangle$ and $|\bar{b}\rangle$. Clearly the energy of state $|e\rangle$ remains the same. The off-diagonal elements represent direct couplings between the states. $H_{-e} = 0$, which means that the $|-\rangle$ state is not directly coupled to the $|e\rangle$ state, independent of the values of the parameters. Physically, this decoupling occurs because the states $|\bar{a}\rangle$ and $|\bar{b}\rangle$ are out of phase, so that the dipole moments coupling these states to state $|\bar{e}\rangle$ cancel each other. On the other hand, in the case of the $|+\rangle$ state these dipole moments add, yielding a strong coupling between $|+\rangle$ and $|e\rangle$, so that $H_{+e} = -\hbar g/2$. Next, note that the $|-\rangle$ and $|+\rangle$ states are coupled as well, at the rate of $H_{-+} = S\Delta$. To understand this coupling, recall that $|\bar{a}\rangle$ and $|\bar{b}\rangle$ differ in energy by an amount Δ . Thus the $|-\rangle$ state rotates into the $|+\rangle$ state at the same rate, modified by the factor $S = \sin 2\theta$ to account for the different weights of $|\bar{a}\rangle$ and $|\bar{b}\rangle$ in the states $|-\rangle$ and $|+\rangle$. For example, consider the case of $g_1 = g_2$. Here $|-\rangle = (1/\sqrt{2})(|\bar{a}\rangle - |\bar{b}\rangle)$ and $|+\rangle = (1/\sqrt{2})(|\bar{a}\rangle + |\bar{b}\rangle)$. So if $|\psi(t=0)\rangle = |-\rangle$, then, ignoring any field-induced couplings, $|\psi(t)\rangle = (1/\sqrt{2})(|\bar{a}\rangle e^{-i\Delta t/2} - |\bar{b}\rangle e^{+i\Delta t/2}) \propto (|\bar{a}\rangle - |\bar{b}\rangle) e^{i\Delta t}$. Thus, after a time π/Δ , $|\psi\rangle$ will equal $|+\rangle$. If $S\Delta = 0$, the $|-\rangle$ state is also decoupled from $|+\rangle$ state, so that in steady state, all of the population is in the trapped state. This occurs either when $\Delta = 0$ or when $g_1 = 0$ ($g_2 = 0$), which corresponds to $|-\rangle = |\bar{a}\rangle$ ($|-\rangle = |\bar{b}\rangle$), i.e., simple optical pumping into one of the ground states.

Consider next the elements of the source matrix. When an atom decays from $|\bar{e}\rangle$ to $|\bar{a}\rangle$, for example, it adds to the populations of both states $|-\rangle$ and $|+\rangle$, as well as to the coherence ρ_{-+} between these two states. Explicitly, $|\bar{a}\rangle = \cos\theta|-\rangle + \sin\theta|+\rangle$, so that the decay to state $|\bar{a}\rangle$ contributes $\Gamma_{ea}\cos^2\theta$ to ρ_{--} , $\Gamma_{ea}\sin^2\theta$ to ρ_{++} , and $\Gamma_{ea}\sin 2\theta/2$ to ρ_{-+} . Similarly, the decay to state $|\bar{b}\rangle = -\sin\theta|-\rangle + \cos\theta|+\rangle$ contributes $\Gamma_{eb}\sin^2\theta$ to ρ_{--} , $\Gamma_{eb}\cos^2\theta$ to ρ_{++} , and $-\Gamma_{eb}\sin 2\theta/2$ to ρ_{-+} . The elements of S simply represent the algebraic sum of these two sets of contributions. In particular, note that the sources to the coherence ρ_{-+} exactly cancel each other only if $\Gamma_{ea} = \Gamma_{eb}$, i.e., $d = 0$. When $d \neq 0$, spontaneous emission does add to the coherence ρ_{-+} . For simplic-

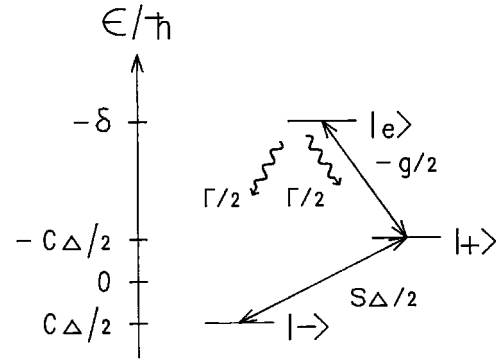


FIG. 2. A system under Raman excitation in terms of the partially diagonalized basis states. Shown are the coupling strengths, the decay rates for the case $d=0$ (i.e., $\Gamma_{ea} = \Gamma_{eb}$), and the relative energies for the case $\Delta < 0$ and $\delta < 0$. Note that the trapped state $|-\rangle$ is not directly coupled to the excited state $|e\rangle$, but is indirectly coupled to $|e\rangle$ through the $|+\rangle$ state.

ity, we consider the case of equal decay rates ($\Gamma_{ea} = \Gamma_{eb} = \Gamma/2$) for most of this paper.

The density-matrix equation of motion [Eq. (11)] is illustrated graphically in Fig. 2, for negative values of δ and Δ . When Eq. (11) is expanded, subject to the constraint that $\rho_{--} + \rho_{++} + \rho_{ee} = 1$ (i.e., a closed system), we get eight linearly independent differential equations. The time-dependent solution of these equations can be found, for example, by numerical methods. However, for weak interactions ($g \ll \Gamma$), it is possible to find an approximate analytical time-dependent solution quite easily, as we now show.

C. The adiabatic following approximation

The adiabatic following approximation reduces (from 8 to 3) the number of variables needed to describe the state of the system so that the time-dependent solution of the equation of motion can be represented by the motion of a three-element vector in space. The physical idea behind the adiabatic following approximation is that if the decay rate Γ of the excited state is much greater than any of the other parameters in the system, then for any change in the ground states (which occurs on a time scale much greater than $1/\Gamma$), the excited state will rapidly come into equilibrium with the ground states (at the rate of Γ). Thus the excited-state amplitude will adiabatically follow the ground-state amplitudes. That is, the excited-state amplitude (and thus population) will be related to the ground-state amplitudes by some fixed ratio for any time scale greater than $1/\Gamma$. Once that fixed ratio is calculated, the excited state can be eliminated from the equation of motion. The reduced system involves only the two ground states, so that the motion can then be described with only three real variables, which can be modeled by the motion of a three-element vector in space. Thus the time evolution of the entire system can be described by the motion of a vector that can provide simple physical interpretations of the time evolution.

This interpretation is often the simplest in the partially diagonalized ($|-\rangle, |+\rangle, |e\rangle$) basis. We can represent the system for an individual atom by a wave function of the form

$$|\psi\rangle = A_-|-\rangle + A_+|+\rangle + A_e|e\rangle. \quad (15)$$

For a weak interaction ($g \ll \Gamma$), the excited-state population is small (proportional to g^2/Γ^2), so that we can ignore the influx of atoms from the excited state to the ground states. The time evolution of the state amplitudes is given by

$$\begin{bmatrix} \dot{A}_- \\ \dot{A}_+ \\ \dot{A}_e \end{bmatrix} = \frac{1}{2i} \begin{bmatrix} C\Delta & S\Delta & 0 \\ S\Delta & -C\Delta & -g \\ 0 & -g & -2\delta - i\Gamma \end{bmatrix} \begin{bmatrix} A_- \\ A_+ \\ A_e \end{bmatrix}. \quad (16)$$

Here $|-\rangle$ and $|+\rangle$ couple to each other at the rate of $S\Delta/2$, $|+\rangle$ and $|e\rangle$ couple at the rate of $g/2$, and $|e\rangle$ decays at the rate of $\Gamma/2$. With $\Gamma \gg g, S\Delta$, for any change in $|+\rangle$ (which can occur only at the two coupling rates of g and $S\Delta$), $|e\rangle$ comes into equilibrium with $|+\rangle$ at the much faster rate of Γ . For a time greater than $1/\Gamma$, we can then assume that $\dot{A}_e \ll \Gamma A_e$, which implies, from the third line in Eq. (16), that

$$A_e \approx i \frac{g}{\Gamma - i2\delta} A_+. \quad (17)$$

That is, $|e\rangle$ follows $|+\rangle$ with the ratio of Eq. (17). Thus we can eliminate $|e\rangle$ by defining the damped state

$$|+\rangle_d \equiv |+\rangle + i \frac{g}{\Gamma - i2\delta} |e\rangle. \quad (18)$$

The wave function can then be written as

$$|\psi\rangle = A_- |-\rangle + A_+ |+\rangle + A_e |e\rangle = A_- |-\rangle + A_+ |+\rangle_d. \quad (19)$$

Equation (16) is then reduced to

$$i\hbar \begin{bmatrix} \dot{A}_- \\ \dot{A}_+ \end{bmatrix} = H \begin{bmatrix} A_- \\ A_+ \end{bmatrix}, \quad (20)$$

with the Hamiltonian expressed in the $|-\rangle, |+\rangle_d$ basis:

$$H = \frac{\hbar}{2} \begin{bmatrix} C\Delta & S\Delta \\ S\Delta & -C\Delta - i \frac{g^2}{\Gamma - i2\delta} \end{bmatrix}. \quad (21)$$

We define

$$\alpha \equiv \frac{1}{2} \frac{g^2 \Gamma}{\Gamma^2 + 4\delta^2} = \left| \frac{g}{\Gamma - i2\delta} \right|^2 \frac{\Gamma}{2}, \quad (22)$$

$$\beta \equiv \frac{g^2 \delta}{\Gamma^2 + 4\delta^2} = \left| \frac{g}{\Gamma - i2\delta} \right|^2 \delta, \quad (23)$$

so that Eq. (21) becomes

$$H = \frac{\hbar}{2} \begin{bmatrix} C\Delta & S\Delta \\ S\Delta & -(C\Delta - 2\beta) - i2\alpha \end{bmatrix}, \quad (24)$$

i.e., $|+\rangle_d$ has energy of $\hbar(-C\Delta/2 + \beta)$ and a damping rate of α . When compared to $|+\rangle$, the decay rate and the additional energy for $|+\rangle_d$ result from the fraction of $|e\rangle$ that is in $|+\rangle_d$. To see this explicitly, note that (setting $\hbar=1$)

$$\begin{aligned} {}_d\langle +|H|+\rangle_d &= \langle +|H|+\rangle + \left| \frac{g}{\Gamma - i2\delta} \right|^2 \langle e|H|e\rangle \\ &+ 2 \operatorname{Re} \left[\langle +|H|e\rangle \frac{g}{\Gamma - i2\delta} \right] = -\frac{C\Delta}{2} + \beta - i\alpha, \end{aligned} \quad (25)$$

in agreement with Eq. (24). To see it more intuitively, refer to Eqs. (17), (22), and (23). The energy $\hbar\beta$ and decay rate α are just the energy $-\hbar\delta$ and decay rate Γ of $|e\rangle$ multiplied by the factor $g^2/(\Gamma^2 + 4\delta^2) = |g/(\Gamma - i2\delta)|^2$, which is simply the proportion of state $|e\rangle$ in state $|+\rangle_d$ [Eq. (17)].

In deriving Eq. (17), we ignored the influx of atoms from state $|e\rangle$ to $|+\rangle$, since for small values of g ($g \ll \Gamma$), ρ_{ee} is small, making $\Gamma\rho_{ee} \ll \rho_{++}$. For the reduced system of $|-\rangle$ and $|+\rangle_d$, however, we want to consider the general situation in which the $|-\rangle \leftrightarrow |+\rangle_d$ coupling can possibly be as large as the decay rate of $|+\rangle_d$. In such a situation, the source terms can no longer be ignored, and we must return to the density-matrix formulation for the equation of motion. In the new $|-\rangle, |+\rangle_d$ basis, we have

$$\dot{\rho} = \frac{i}{\hbar} [\rho H^\dagger - H\rho] + L\rho_{++}. \quad (26)$$

Here

$$\rho = \begin{bmatrix} \rho_{--} & \rho_{-+} \\ \rho_{+-} & \rho_{++} \end{bmatrix}, \quad L = \begin{bmatrix} \alpha & 0 \\ 0 & \alpha \end{bmatrix}, \quad (27)$$

where we have used $\rho_{ee} = \rho_{++} g^2/(\Gamma^2 + 4\delta^2)$, and

$$H = \frac{\hbar}{2} \begin{bmatrix} -\beta' & S\Delta \\ S\Delta & \beta' - i2\alpha \end{bmatrix}, \quad (28)$$

which is the same as in Eq. (24), except that we have subtracted an energy of $\hbar\beta/2$ from the diagonal to make it more symmetric and have defined $\beta' \equiv \beta - C\Delta$. Note that $\hbar\beta'$ equals the energy difference between the states $|+\rangle_d$ and $|-\rangle$. Also note that $|-\rangle$ and $|+\rangle_d$ are coupled at the rate of $S\Delta/2$, which is just the coupling between the $|-\rangle$ state and the (predominant) $|+\rangle$ part of $|+\rangle_d$. Note that atoms decaying from the $|+\rangle_d$ state go to both states $|-\rangle$ and $|+\rangle_d$. This is as expected, since the decay of $|+\rangle_d$ is due to the decay of state $|e\rangle$ to both $|-\rangle$ and $|+\rangle$ (equally, in the case of $\Gamma_{ea} = \Gamma_{eb}$).

III. THE THREE-ELEMENT BLOCH VECTOR MODEL

A. The Bloch vector equation of motion

We now define a three-element Bloch vector to pictorially describe the time evolution of the Λ system under Raman excitation as expressed by the density-matrix equation of motion [Eq. (26)]. We define the three-element Bloch vector

$$\mathbf{R} \equiv R_1 \hat{\mathbf{e}}_1 + R_2 \hat{\mathbf{e}}_2 + R_3 \hat{\mathbf{e}}_3, \quad (29)$$

where $\hat{\mathbf{e}}_i$ are abstract unit vectors and the three real elements are defined as

$$\frac{1}{2}(R_1 + iR_2) \equiv \rho_{-+}, \quad R_3 \equiv (\rho_{--} - \rho_{++}). \quad (30)$$

This definition is motivated by an analogy with the two-level (spin- $\frac{1}{2}$) system Bloch vector. Within the adiabatic following limit, these three elements can be used to compute all nine density-matrix elements, and thus all observables, in the interaction. Using the constraint that $\rho_{--} + \rho_{++} = 1$, we get

$$\rho_{--} = \frac{1}{2}(1 + R_3), \quad \rho_{++} = \frac{1}{2}(1 - R_3). \quad (31)$$

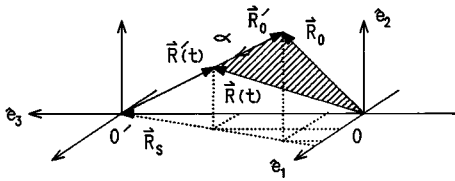


FIG. 3. Motion of the three-element Bloch vector for the case $S\Delta=0$, $\beta'=0$, $\alpha\neq 0$ (i.e., decay only). The initial offset Bloch vector (OBV) \mathbf{R}'_0 decays in a straight line to the steady-state value zero at the rate of α . The corresponding Bloch vector (BV) decays from \mathbf{R}_0 to $\mathbf{R}_S=1\hat{\mathbf{e}}_3$, i.e., all the atoms in the trapped state. The axes $\hat{\mathbf{e}}_1$, $\hat{\mathbf{e}}_2$, $\hat{\mathbf{e}}_3$ centered at the origin O represent $2\text{Re}\rho_{-+}$, $2\text{Im}\rho_{-+}$, and $(\rho_{--}-\rho_{++})$, respectively.

To find observables involving the state $|e\rangle$, we use Eq. (17) to get

$$\rho_{ee} = \frac{\alpha}{\Gamma} (1-R_3), \quad \rho_{e+} = \frac{-\beta+i\alpha}{g} (1-R_3),$$

$$\rho_{e-} = \frac{-\beta+i\alpha}{g} (R_1-iR_2). \quad (32)$$

Equations (30)–(32) express all the elements of the partially diagonalized states density matrix (ρ) in terms of the three elements of the Bloch vector.

The equation of motion for the Bloch vector is simply found by expanding Eq. (26) to give

$$\begin{bmatrix} \dot{R}_1 \\ \dot{R}_2 \\ \dot{R}_3 \end{bmatrix} = \begin{bmatrix} -\alpha & -\beta' & 0 \\ \beta' & -\alpha & S\Delta \\ 0 & -S\Delta & -\alpha \end{bmatrix} \begin{bmatrix} R_1 \\ R_2 \\ R_3 \end{bmatrix} + \begin{bmatrix} 0 \\ 0 \\ \alpha \end{bmatrix}. \quad (33)$$

Again, this equation holds in the adiabatic following limit and for the case of $\Gamma_{ea}=\Gamma_{eb}$ ($d=0$). It can be expressed in the form

$$\dot{\mathbf{R}} = \mathbf{Q} \times \mathbf{R} - \alpha \mathbf{R} + \alpha \hat{\mathbf{e}}_3, \quad (34)$$

where \mathbf{Q} is the torque vector, given by

$$\mathbf{Q} = -S\Delta \hat{\mathbf{e}}_1 + \beta' \hat{\mathbf{e}}_3. \quad (35)$$

The Bloch vector equation of motion [Eq. (34)] reflects two types of motion: precession of \mathbf{R} about \mathbf{Q} at the rate of $|\mathbf{Q}|$ and decay of \mathbf{R} to some equilibrium position (to be calculated later) at the rate of α . To understand this motion in physical terms, consider each of the three parameters in Eq. (34): $S\Delta$, β' , and α , separately.

In the case of no decay ($\alpha=0$), there is a strict analogy between the behavior of this system and that of the undamped two-level system. $S\Delta$ represents the coupling between the $|-\rangle$ and $|+\rangle_d$ states and is analogous to the Rabi frequency. β' represents the energy difference between the $|-\rangle$ and $|+\rangle_d$ states and is analogous to the two-level system detuning (i.e., the energy difference between the two states in the rotating frame). Thus, if $\alpha=0$, $\beta'=0$, and $S\Delta\neq 0$, then $\mathbf{Q} = -S\Delta \hat{\mathbf{e}}_1$. The effect of \mathbf{Q} is to mix R_2 and R_3 , which represent $2\text{Re}\rho_{-+}$ and $\rho_{--}-\rho_{++}$, respectively, at the rate of the $|-\rangle \leftrightarrow |+\rangle_d$ coupling. This population flipping is just

the familiar Rabi flopping in the two-level system. Similarly, if $\alpha=0$, $\beta'\neq 0$, and $S\Delta=0$, then $\mathbf{Q} = \beta' \hat{\mathbf{e}}_3$. The effect of \mathbf{Q} is to mix R_1 and R_2 , which represent $2\text{Re}\rho_{-+}$ and $2\text{Im}\rho_{-+}$, respectively, at the rate of the $|-\rangle \leftrightarrow |+\rangle_d$ energy difference (“detuning”), while the initial population difference is conserved. This is simply a manifestation of the dephasing between $|-\rangle$ and $|+\rangle_d$ and is also familiar from two-level systems. In general, when $S\Delta$ and β' are both nonzero, \mathbf{Q} acts just as the effective Rabi frequency vector in the two-level case.

Consider next the effect of α , the decay rate of $|+\rangle_d$. The second term of Eq. (34) indicates that each element of the Bloch vector \mathbf{R} , decays at this rate. But, at the same time, the third element of the Bloch vector grows at the rate of α , as indicated by the third term in Eq. (34). To understand the net effect of these two processes, consider first the simplest case in which $|\mathbf{Q}|=0$. As can be seen by inspection from Eq. (34), the Bloch vector then decays to the steady-state value (found by setting $\dot{\mathbf{R}}=0$) of $\mathbf{R}_S=1\hat{\mathbf{e}}_3$, i.e., $R_{1S}=0$, $R_{2S}=0$, and $R_{3S}=1$, corresponding to $\rho_{-+}=\rho_{++}=0$ and $\rho_{--}=1$. Physically, this means that all the atoms have been pumped into the trapped state. This occurs because we have set $S\Delta=0$, meaning that the $|-\rangle$ state is completely decoupled from the system. In general, however, \mathbf{R}_S is not equal to $1\hat{\mathbf{e}}_3$. Its value is a balance of the three motions discussed above (due to $S\Delta$, β' , and α) and is given by setting $\dot{\mathbf{R}}=0$ in Eq. (34). We get

$$\mathbf{Q} \times \mathbf{R}_S - \alpha (\mathbf{R}_S - \hat{\mathbf{e}}_3) = 0. \quad (36)$$

The explicit expression is

$$\mathbf{R}_S = \begin{bmatrix} R_{1S} \\ R_{2S} \\ R_{3S} \end{bmatrix} = \frac{1}{\alpha^2 + \beta'^2 + (S\Delta)^2} \begin{bmatrix} -\beta' S\Delta \\ \alpha S\Delta \\ \alpha^2 + \beta'^2 \end{bmatrix}. \quad (37)$$

Now, since it is more natural to picture a vector decaying to zero instead of to some other constant vector, we define the offset Bloch vector \mathbf{R}'

$$\mathbf{R}' \equiv \mathbf{R} - \mathbf{R}_S. \quad (38)$$

This has the effect of shifting the origin to the position of \mathbf{R}_S , so that the offset Bloch vector will decay to zero (with respect to this new origin) in the steady state. Using Eqs. (34), (36), and (38), we can see this explicitly in the offset Bloch vector equation of motion

$$\dot{\mathbf{R}}' = \mathbf{Q} \times \mathbf{R}' - \alpha \mathbf{R}'. \quad (39)$$

Thus the offset Bloch vector (OBV) rotates around the same \mathbf{Q} as the Bloch vector itself, while simply decaying to zero amplitude at the rate of α . This is illustrated in Fig. 3 for $|\mathbf{Q}|=0$.

There is one final point to make before applying this model to specific problems. Equations (30)–(32) express all the elements of the partially diagonalized states density matrix (ρ) in terms of the three elements of the Bloch vector. Under certain circumstances, however, one needs to know explicitly the elements of the atomic states density matrix

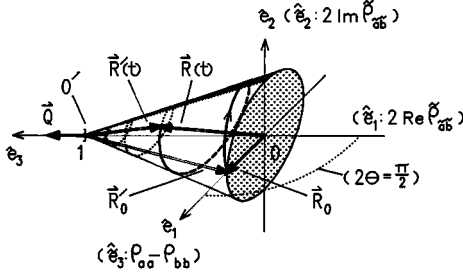


FIG. 4. Motion of the BV for the case $S\Delta=0$, $\beta' \neq 0$, $\alpha \neq 0$, with initial condition $\mathbf{R}_0=R_{10}\hat{\mathbf{e}}_1$. As one can see, the motion of the OBV \mathbf{R}' is much simpler. It consists of precession about the torque vector $\mathbf{Q}=\beta'\mathbf{e}_3$ at the rate of $|\mathbf{Q}|=|\beta'|$ and decay at the rate of α to the steady-state value $\mathbf{R}'=0$ ($\mathbf{R}=\hat{\mathbf{e}}_3$) corresponding to $\rho_{--}=1$. The time evolution of the OBV forms a spiral on a cone of evolution. The terms in parentheses give the motion in terms of the atomic states for the condition $g_1=g_2$. For different ratios of g_1/g_2 (keeping g constant), only the rotation angle 2θ will change, thus illustrating the ease with which the Bloch vector model in the partially diagonalized basis handles unequal Rabi frequencies.

($\tilde{\rho}$). For example, in our experiment (to be described later) involving Raman excitation followed by a microwave excitation, and vice versa, it is important to know, for example, the coherence and population difference between states $|\tilde{a}\rangle$ and $|\tilde{b}\rangle$. In general, the initial conditions and observables are often best expressed in terms of the elements of the atomic state density matrix.

The partially diagonalized state density matrix contains all the information of the atomic state density matrix, related through Eq. (12). If we define

$$\frac{1}{2}(\tilde{R}_1 + i\tilde{R}_2) \equiv \tilde{\rho}_{\tilde{a}\tilde{b}}, \quad \tilde{R}_3 \equiv (\tilde{\rho}_{\tilde{a}\tilde{a}} - \tilde{\rho}_{\tilde{b}\tilde{b}}) = (\rho_{aa} - \rho_{bb}), \quad (40)$$

then the original Bloch vector \mathbf{R} gives these components directly:

$$\mathbf{R} = \tilde{R}_1\hat{\mathbf{e}}_1 + \tilde{R}_2\hat{\mathbf{e}}_2 + \tilde{R}_3\hat{\mathbf{e}}_3, \quad (41)$$

where the $\hat{\mathbf{e}}_i$ basis is related to the $\tilde{\mathbf{e}}_i$ basis by a simple rotation of 2θ in the 1-3 plane. Specifically, to get the $\tilde{\mathbf{e}}_i$ basis, rotate counterclockwise from the $\hat{\mathbf{e}}_i$ basis through 2θ . That is,

$$\begin{bmatrix} \tilde{R}_1 \\ \tilde{R}_2 \\ \tilde{R}_3 \end{bmatrix} = \begin{bmatrix} C & 0 & -S \\ 0 & 1 & 0 \\ S & 0 & C \end{bmatrix} \begin{bmatrix} R_1 \\ R_2 \\ R_3 \end{bmatrix}. \quad (42)$$

Pictorially, given the position of the Bloch vector \mathbf{R} at any time, one simply has to project the vector onto the $\tilde{\mathbf{e}}_i$ axes in order to get the atomic state density-matrix elements. For instance, if $g_1=0$, then from $\sin\theta=g_1/g$ we find that $\theta=0$. Thus the partially diagonalized basis and atomic state basis coincide, which is expected, since in this case $|\tilde{a}\rangle$ is the trapped state $|-\rangle$.

Now consider the previous case of $S\Delta=0$, $\beta' \neq 0$, and $\alpha \neq 0$, with the initial condition $\mathbf{R}_0=R_{10}\hat{\mathbf{e}}_1$ (pictured in Fig. 4). In particular, consider the case in which the Raman interaction satisfies the condition $g_1=g_2$ (i.e., equal Rabi frequencies) at all times. Again using $\sin\theta=g_1/g$, this implies

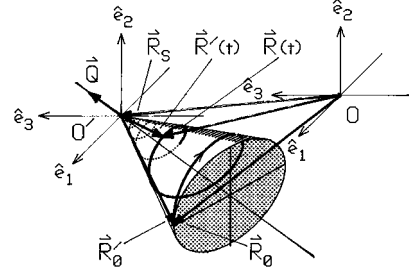


FIG. 5. Construction of the Bloch vector model for the most general values of the parameters $S\Delta$, β' , α , and \mathbf{R}_0 .

that $\theta=\pi/4$ and thus that the atomic state basis and partially diagonalized basis are rotated by $\pi/2$ in the 1-3 plane with respect to each other (see Fig. 4). Therefore, the initial condition is equivalent to $\mathbf{R}_0=R_{10}\hat{\mathbf{e}}_3$. That is, the initial population difference $\tilde{\rho}_{\tilde{a}\tilde{a}}-\tilde{\rho}_{\tilde{b}\tilde{b}}$ equals $R_{10}=\tilde{R}_{30}$. The explicit equation of motion in terms of the atomic state components can easily be found by solving Eq. (39) and then using Eq. (42). If the Raman interaction had $g_1 \neq g_2$, but gave rise to the same values for $S\Delta$, β' , and α (in particular, the values of Δ , δ , Γ , and g^2 were the same), then the same picture would apply, except with rotation of the axes through a different value of 2θ . That is, the Bloch vector picture in terms of the partially diagonalized basis would remain exactly the same. This illustrates one of the key advantages of the Bloch vector model: it is equally simple for all ratios of Rabi frequencies (g_1/g_2). This aspect will be exploited in the modeling of low-intensity adiabatic passage.

Regardless of whether or not one needs to use the atomic state basis, the partially diagonalized basis is always the one in which the Bloch vector model is best constructed, for as we have shown above, it has a simple form and physical interpretation there. The following will be a step-by-step construction of a full Bloch vector model for arbitrary values of the parameters (see Fig. 5). Start with the atomic states basis $\tilde{\mathbf{e}}_i$ (not shown), with origin at O . Calculate θ from the given values of g_1 and g_2 . Rotate the axes clockwise by 2θ in the 1-3 plane to get the partially diagonalized basis $\hat{\mathbf{e}}_i$ (shown at the upper right corner of Fig. 5). Given the initial population difference and coherence, place the initial Bloch vector \mathbf{R}_0 (using either basis). From this point on, use the partially diagonalized basis only. Now calculate the steady-state vector \mathbf{R}_S [Eq. (37)] from the calculated values of $S\Delta$, β' , and α . Translate the partially diagonalized basis to the offset Bloch vector origin O' , which lies at the tip of \mathbf{R}_S . Now place the torque vector \mathbf{Q} at O' [Eq. (35)]. Place the initial OBV \mathbf{R}'_0 at O' , connecting its tip to that of \mathbf{R}_0 . Now draw the cone of evolution, the surface of revolution of \mathbf{R}'_0 about the axis that contains \mathbf{Q} . The time evolution of the system is represented by an exponentially decaying spiral on the surface of the cone [Eq. (39)]. The Bloch vector at any time t , $\mathbf{R}(t)$, is just the vector with origin at O and tip at $\mathbf{R}'(t)$. The values of R_i or \tilde{R}_i can be read off by projecting $\mathbf{R}(t)$ onto the partially diagonalized or atomic states basis (both with origin at O), respectively.

IV. APPLICATIONS OF THE BLOCH VECTOR MODEL

We now illustrate the simplicity and power of the Bloch vector model by describing a few systems of interest.

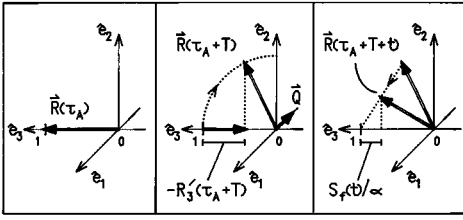


FIG. 6. Two-zone Raman interaction that leads to the generation of Raman-Ramsey fringes. Displayed is the ideal case in which there is no ac Stark shift of the central minimum. For all zones, $\beta' = 0$. An atomic beam first passes through zone A excitation for time τ_A . $|S\Delta| \ll \alpha$ and $\alpha\tau_A \gg 1$, so the system reaches the steady-state value $\mathbf{R}(\tau_A) = \mathbf{R}_S = 1\hat{\mathbf{e}}_3$, with all the atoms in the trapped state. Then the atomic beam passes through the dark zone with no excitation for time T . Now $\alpha = 0$, so the BV precesses without decay about $\mathbf{Q} = -S\Delta\hat{\mathbf{e}}_1$ for time T , sweeping out an angle $S\Delta T$. Finally, the atomic beam passes through the zone B excitation. Again $|S\Delta| \ll \alpha$, so the BV decays to $\mathbf{R}_S = 1\hat{\mathbf{e}}_3$ at a rate of α . The resulting integrated observed fluorescence in zone B as a function of $S\Delta$ gives the Raman-Ramsey fringes.

A. The ac Stark shift in Raman-Ramsey fringes

In the application of Raman-Ramsey fringes to atomic clocks, the ac Stark shift (seen as a shift in the Ramsey central minimum) is a direct source of error [3]. Before we explain this shift in terms of the Bloch vector model, we must first express our observable, fluorescence, in terms of Bloch vector components. Then we can describe the generation of the fringes and, afterward, the shift.

The fluorescence signal S_f is proportional to the excited-state population ρ_{ee} . From the adiabatic following approximation [in particular, Eq. (17)], we have

$$\rho_{ee} = \left| \frac{g}{\Gamma - i2\delta} \right|^2 \rho_{++}. \quad (43)$$

Thus

$$S_f \equiv \Gamma \rho_{ee} = 2\alpha \rho_{++} = \alpha(1 - R_3), \quad (44)$$

where the last step is from Eq. (31).

First we will describe the generation of the ideal Raman-Ramsey fringes, in which the central minimum occurs at $\Delta = 0$. The two-zone Raman interaction that generates the Raman-Ramsey fringes consists of an atomic beam that passes through three regions in succession: first Raman excitation in zone A for a time τ_A , next a dark zone with no fields for a time T , and finally Raman excitation in zone B, which is identical to that in zone A (Fig. 6). We assume that $\beta' = 0$ and $|S\Delta| \ll \alpha$ in both excitation zones. Thus $\mathbf{R}_S = 1\hat{\mathbf{e}}_3$ [Eq. (37)], i.e., all atoms in the trapped state. For now, we assume that the zone A interaction is strong enough so that $\alpha\tau_A \gg 1$, i.e., that the system reaches steady state by the end of zone A: $\mathbf{R}(\tau_A) = 1\hat{\mathbf{e}}_3$. In the dark zone, $\alpha \propto g^2 = 0$ (since $g = 0$ there), thus we can no longer ignore $S\Delta$. This causes the Bloch vector to precess (Rabi flopping) at the rate of $S\Delta$, so that during the dark zone flight time T , \mathbf{R} rotates through an angle $S\Delta T$. At the end of the dark zone, we have by inspection

$$\mathbf{R}(\tau_A + T) = \sin(S\Delta T)\hat{\mathbf{e}}_2 + \cos(S\Delta T)\hat{\mathbf{e}}_3. \quad (45)$$

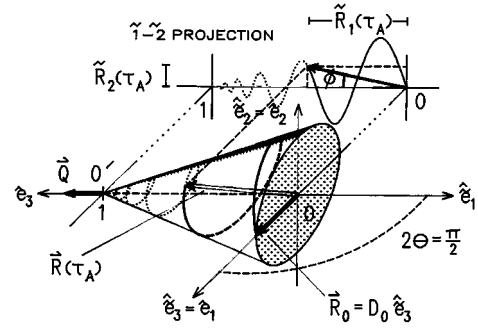


FIG. 7. ac Stark shift in the generation of Raman-Ramsey fringes in a two-zone interaction. This time β is not necessarily zero in excitation zones. An atomic beam first passes through zone A excitation for time τ_A . $|\Delta| \ll \alpha, |\beta|$, so the BV precesses and decays toward the steady-state value $\mathbf{R}_S = 1\hat{\mathbf{e}}_3$ until it leaves zone A at $\mathbf{R}(\tau_A)$. Note that the BV does not necessarily reach the steady state in zone A, unlike in Fig. 6. This leads to the shift of the fringe central minimum.

We assume that the fields have the same phases in zone B as in zone A, so that we can simply continue with $\mathbf{R}(\tau_A + T)$ in the same position as in the dark zone. In zone B, $|S\Delta| \ll \alpha$, so $\mathbf{R}_S = 1\hat{\mathbf{e}}_3$ again and we assume that $\mathbf{Q} = -S\Delta\hat{\mathbf{e}}_1$ is negligible. The OBV just decays linearly to \mathbf{R}_S . The fluorescence at any time t is simply given by Eqs. (44) and (45):

$$S_f(t) = \alpha[1 - \cos(S\Delta T)]e^{-\alpha t}. \quad (46)$$

In a typical experiment, the fluorescence observed is integrated over the interaction zone. Thus, for $\alpha\tau_B \gg 1$,

$$\begin{aligned} \overline{S_f} &= \int_0^{\tau_B} dt \alpha[1 - \cos(S\Delta T)]e^{-\alpha t} = 1 - \cos(S\Delta T) \\ &= -R_3'(\tau_A + T), \end{aligned} \quad (47)$$

where the last step is by inspection (Fig. 7). Thus plotting $\overline{S_f}$ as a function of $S\Delta$, i.e.,

$$\overline{S_f}(S\Delta) = 1 - \cos(S\Delta T), \quad (48)$$

generates the ideal Raman-Ramsey fringes, with a minimum of fluorescence at $S\Delta = 0$.

The ac Stark shift in the two-zone setup is the result of less-than-ideal conditions, namely, the fact that the system does not reach equilibrium in zone A and that $\beta' \neq 0$. The term ‘‘ac Stark shift’’ itself refers to the energy difference between the $|-\rangle$ and $|+\rangle_d$ states (β') due to the value of δ ($\beta' \propto \delta$). We will find that there is no shift if $\beta' = 0$. For simplicity, we choose $g_1 = g_2$ in both excitation zones, so that $\theta = \pi/4$. This means that $\beta' = \beta$, $S\Delta = \Delta$, and the partially diagonalized basis is rotated by $\pi/2$ with respect to the atomic states basis. In both excitation zones, we assume that $|\Delta| \ll \alpha, |\beta|$ since we want to consider only a small shift with respect to Δ . Thus $\mathbf{R}_S = 1\hat{\mathbf{e}}_3$ there [Eq. (37)]. In the dark zone, $\alpha = \beta = 0$ (since $g = 0$), so Δ is no longer negligible. This time we choose a specific initial condition $\mathbf{R}_0 = D_0\hat{\mathbf{e}}_3 = D_0\hat{\mathbf{e}}_1$, where $D_0 = \tilde{\rho}_{\tilde{a}\tilde{a}} - \tilde{\rho}_{\tilde{b}\tilde{b}}$ is the initial atomic ground-state population difference. In zone A, the OBV precesses and decays until time τ_A (Fig. 7). We use the $\tilde{1}-\tilde{2}$ projection to calculate the projection angle ϕ by inspection. We have

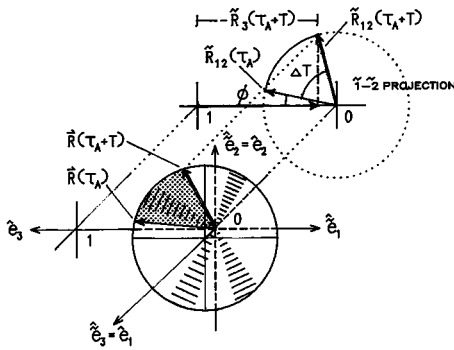


FIG. 8. Dark zone with no excitation for time T . Now $\beta=0$, $\alpha=0$, so the BV precesses without decay about $\mathbf{Q}=-\Delta\hat{\mathbf{e}}_1$ for time T , sweeping out an angle ΔT as seen in the $\bar{1}-\bar{2}$ projection. The integrated observed fluorescence measured in the following zone B is given by the value $-\tilde{R}_3(\tau_A+T)$. Thus the minimum fluorescence occurs for $\Delta=-\phi/T$.

$$\tilde{R}_1(\tau_A) = 1 - e^{-\alpha\tau_A}, \quad \tilde{R}_2(\tau_A) = D_0 e^{-\alpha\tau_A} \sin(\beta\tau_A). \quad (49)$$

Thus

$$\tan \phi = \frac{\tilde{R}_2(\tau_A)}{\tilde{R}_1(\tau_A)} = D_0 \frac{e^{-\alpha\tau_A}}{1 - e^{-\alpha\tau_A}} \sin(\beta\tau_A). \quad (50)$$

In the dark zone, with only $\Delta \neq 0$, the Bloch vector precesses (with constant amplitude) through an angle ΔT (Fig. 8). As shown above, the integrated fluorescence measured in zone B is given by $\bar{S}_f = -R'_3(\tau_A+T)$ [Eq. (47)]. Thus, by inspection, we find that the minimum \bar{S}_f occurs for $\Delta = -\phi/T$ (see the $\bar{1}-\bar{2}$ projection in Fig. 8). Explicitly, the central minimum occurs at

$$\Delta_0 = -\frac{1}{T} \tan^{-1} \left(D_0 \frac{e^{-\alpha\tau_A}}{1 - e^{-\alpha\tau_A}} \sin(\beta\tau_A) \right), \quad (51)$$

where we have used Eq. (50). This ac Stark shift is manifested in the Raman-Ramsey fringes (Fig. 9). Consider now the limiting cases of Eq. (51). For $\alpha\tau \gg 1$, $\Delta_0=0$ since the system reaches equilibrium (all atoms in the trapped state) in zone A , which reduces the case to the ideal Raman-Ramsey fringes. For $\beta=0$ (and these particular initial conditions), the

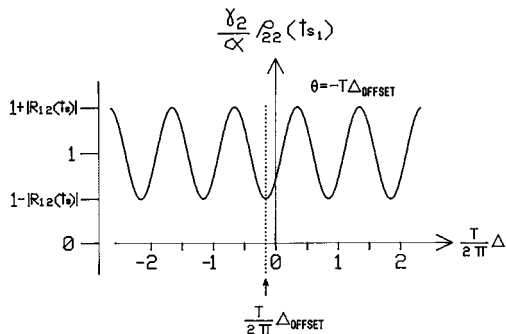


FIG. 9. ac Stark shift. The minimum value of the fluorescence is shifted away from $\Delta=0$ by $-\phi/T$.

ac Stark shift disappears (as can readily be seen from Figs. 7–9). Finally, the shift disappears for $D_0=0$, which is also clear from Figs. 7–9. We point out that in addition to the two-zone interaction described above, the Bloch vector model can be used to derive the Raman dip in the single-zone Raman interaction and its associated ac Stark shift [23].

The Raman clock ac Stark shift predicted by Eq. (51) has been verified quantitatively, over a large range of experimental conditions [3]. In addition, the insight obtained from this derivation was instrumental in identifying conditions for suppressing this effect [3].

B. Separated zone Raman-microwave mixing

The Λ system provides a unique mechanism for mixing optical and microwave fields in particular and widely different frequencies in general. The uniqueness results from the fact that in the presence of two optical frequencies (ω_1 and ω_2), the $|a\rangle \leftrightarrow |b\rangle$ microwave excitation forms a closed loop. As a result, the effect of the interaction depends nontrivially on the phase difference ($\phi_M - \phi_R$), where ϕ_M is the phase of the microwave field and ϕ_R is the phase of the Raman product field (defined as $\phi_R = \phi_1 - \phi_2$, where ϕ_1 and ϕ_2 are the phases of the individual optical fields at frequencies ω_1 and ω_2). To see why, note that, for example, the coherence between states $|a\rangle$ and $|b\rangle$ is excited in two ways: directly by the microwave fields and indirectly by the two optical frequencies. Since each of these two processes tends to drive the coherence at its own phase, there exists a competition between them. The result of this competition therefore depends strongly on the difference between the phases.

This type of interaction has several potential applications. For example, it can be shown that Raman-microwave excitation can be used, with the proper choice of ϕ , to pump atoms selectively into either the strong-field-seeking or the weak-field-seeking dressed state of the microwave excitation. This could potentially be used to make a much higher density trap, which requires atoms in a particular dressed state. Atoms that leave the required state due to phase-changing collisions could be pumped right back [10,24]. Raman-microwave spin echo could possibly be used in optical data storage, with potential advantages over the optical photon echo processes as well as spin echo processes [11]. Finally, such a closed-loop mixing could be used for the ultrahigh-resolution mapping of the phase of, for example, a millimeter-wave field. This is of significant interest in designing components such as a phased array antenna. To illustrate how such a phase mapping can be performed, we discuss now the microwave phase sensitive absorption of the optical beams in the Λ configuration [10].

The separated zone Raman-microwave mixing scheme consists of an atomic beam that passes successively through a Raman-only zone, then a microwave-only zone, and finally another Raman-only zone (Fig. 10). Thus the ground-state coherence is first excited by a Raman pulse. The atoms bearing this coherence then encounter a microwave pulse. The effect of this interaction with the microwave pulse is then determined by probing the atoms again with a Raman pulse. For simplicity, we assume that the two Raman zones are in phase, have $g_1 = g_2$, and leave all atoms in the trapped state in the steady state. In terms of Raman and microwave Bloch vectors, the interaction is very simple to understand. Consider first the case in which the phase difference between the

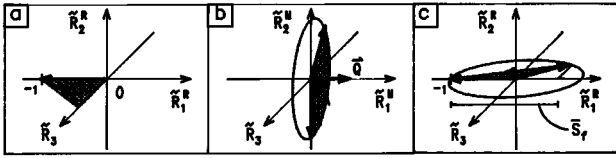


FIG. 10. Separated zone Raman-microwave mixing for the case in which the phase difference between the Raman and microwave fields is $\Delta\phi = \pi/2$. An atomic beam passes successively through a Raman only field, then a microwave only field, and finally another Raman only field. Note the different Raman and microwave bases: $\tilde{R}_3^R = \rho_{aa} - \rho_{bb}$ for both $\tilde{R}_1^R = 2 \text{Re } \rho_{ab}^R$, $\tilde{R}_2^R = 2 \text{Im } \rho_{ab}^R$, and $\tilde{R}_1^M = 2 \text{Re } \rho_{ab}^M$, $\tilde{R}_2^M = 2 \text{Im } \rho_{ab}^M$, where $\rho_{ab}^R = \rho_{ab} e^{i\phi_R}$, $\rho_{ab}^M = \rho_{ab} e^{i\phi_M}$, and $\Delta\phi = \phi_M - \phi_R$. The Raman BV reaches steady state in the first Raman zone. Then the microwave BV is found by rotating the Raman BV by $\Delta\phi$ in the coherence plane ($\tilde{1}$ - $\tilde{2}$ plane). The microwave BV precesses due to microwave excitation about the Rabi frequency vector $\mathbf{Q} = g_3 \hat{e}_1^M$. The Raman BV is found again by rotating back by $\Delta\phi$. The second Raman interaction pumps atoms back into the trapped state and the integrated observed fluorescence \bar{S}_f is measured. In general, \bar{S}_f varies sinusoidally with both the phase and the strength of the microwave field.

microwave zone and the Raman zone is zero ($\Delta\phi = \phi_M - \phi_R = 0$). The Raman interaction in the first zone pumps the system into a perfect trapped state. To go from the first to the second zone, the Raman Bloch vector must be rotated in the coherence plane by the phase difference to become the microwave Bloch vector (BV). This is so because each Bloch vector picture incorporates the relative phases. This phase information is necessary to relate the rotating frame (of the BV) to the atom's frame (i.e., $\rho_{ab}^R = \rho_{ab} e^{i\phi_R} = \rho_{ab} e^{i(\phi_1 - \phi_2)}$ and $\rho_{ab}^M = \rho_{ab} e^{i\phi_M} = \rho_{ab} e^{i\phi_3}$). Since the phase difference is zero in this case, in the second zone the state appears as one of the dressed (stationary) states of the microwave interaction [specifically $|\psi\rangle = (1/\sqrt{2})(|\tilde{a}\rangle - |\tilde{b}\rangle)$], so that the atom appears transparent to the microwave field. When this atom is probed again by the Raman pulse, it exhibits a fluorescence (i.e., \bar{S}_f) minimum, as if the microwave pulse did not occur at all. Consider next the case where $\Delta\phi = \pi/2$. The first zone is the same as in the previous case. But in going from the first to the second zone, the Raman Bloch vector must be rotated by $\pi/2$ to convert it

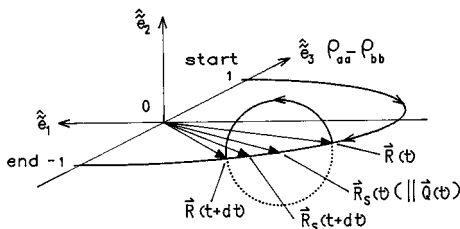


FIG. 11. Low-intensity adiabatic passage explained in terms of the atomic states basis. The motion of the BV is like that of a precessing top. As the equilibrium vector \mathbf{R}_S moves from $1\hat{e}_3$ to $-1\hat{e}_3$, the BV follows it around by precessing about it, rather than decaying to it, resulting in coherent population transfer.

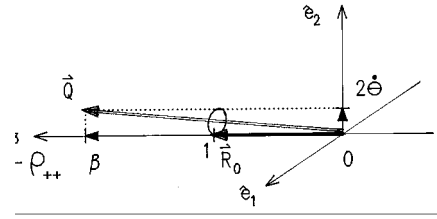


FIG. 12. Low-intensity adiabatic passage in terms of the partially diagonalized basis. If $\beta \gg 2\dot{\theta}$ (and $S\Delta$), then the net precession vector \mathbf{Q} will lie very close to the \hat{e}_3 axis. Thus the initial BV $\mathbf{R}_0 = 1\hat{e}_3$ will stay very close to the dark state at all times as the Rabi frequency ratio is varied. This results in very little excited-state population and thus coherent population transfer from one ground state to the other.

to the microwave Bloch vector. In the microwave Bloch vector picture, the Bloch vector lies in the Rabi-flopping plane (here it appears to be in a state with coherence that is pure negative imaginary) and thus strongly interacts with the microwave field, undergoing Rabi flopping at the rate of g_3 (the microwave Rabi frequency). If the pulse strength corresponds to a multiple of 2π pulses, then again the Raman probe in the third zone yields a fluorescence minimum. For any other value of the microwave pulse size, the atoms no longer appear to be completely in the trapped state in the second Raman zone. As a result, the fluorescence is no longer minimum. In particular, for a π microwave pulse, the atoms appear to be in the strongly absorbing $|+\rangle$ state in the second Raman zone, thus yielding a fluorescence maximum. In general, the fluorescence oscillates sinusoidally with the pulse strength.

For a given pulse strength, such as π , the fluorescence observed is maximum for $\Delta\phi = \pi/2$ and minimum for $\Delta\phi = 0$, as we have just shown. It is simple to show that, in general, the fluorescence varies sinusoidally with both the phase and the field strength of the microwave field. Thus, to use this process for measuring the phase alone with optical resolution, the amplitude must also be measured with equal resolution. Note that this can easily be done by shutting off one of the frequencies of the two Raman beams (e.g., $g_1 = 0$). The experiment then corresponds to normal optical pumping into $|a\rangle$ or $|b\rangle$ in both Raman zones and therefore depends only

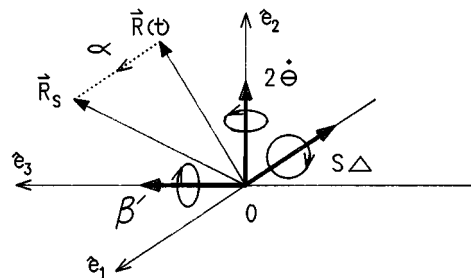


FIG. 13. Summary of the separate contributions to the motion of the Bloch vector $\mathbf{R}(t)$ in the partially diagonalized basis. The overall motion is a balance of the three torques $S\Delta$ ($|-\rangle \leftrightarrow |+\rangle_d$ coupling), β' ($|-\rangle/|+\rangle_d$ energy difference), $2\dot{\theta}$ (rate of change of the Rabi frequency ratio), and the decay rate α . The steady state value is \mathbf{R}_S .

on the amplitude of the microwave field. This situation can be pictured from Fig. 10. Everything would be the same, except the Raman steady state would always be perpendicular to the coherence plane, in which case $\Delta\phi$ would not affect the Bloch vector.

C. Low-intensity adiabatic passage

Adiabatic passage is a process by which population is transferred from one ground state (of the Λ system) to the other *coherently*. Thus, in the ideal case, there should never be any excited-state population throughout the entire process. If at any point there is any excited-state population, spontaneous emission may occur, with atoms falling into the ground states incoherently. In a recent experiment [13,14], population has been transferred with little loss due to spontaneous emission. In the dressed-state Bloch vector picture, ideal adiabatic passage requires that the system be in the trapped state at all times.

The method of transferring population from $|a\rangle$ to $|b\rangle$ is to vary the Rabi frequency ratio from $g_1/g_2=0$ to $g_1/g_2=\infty$ while holding $g=\sqrt{g_1^2+g_2^2}$ constant. So at the beginning, $|-\rangle=|a\rangle$, and at the end, $|-\rangle=|b\rangle$, with $|-\rangle$ passing through intermediate superposition states of $|a\rangle$ and $|b\rangle$. The conditions are chosen so that $\mathbf{R}_S=1\hat{\mathbf{e}}_3$ (i.e., all the atoms are in the $|-\rangle$ state at equilibrium). Thus, for the process to be highly coherent, the system must be near equilibrium at every point throughout the process. In practice, this is accomplished by varying the Rabi frequency ratio very slowly. In terms of the Bloch vector picture in the atomic state basis, the equilibrium vector (which coincides with the $\hat{\mathbf{e}}_3$ axis of the partially diagonalized basis) will be rotated through an angle of π from $\mathbf{R}=1\hat{\mathbf{e}}_3$ to $\mathbf{R}=-1\hat{\mathbf{e}}_3$ (Fig. 11). The Bloch vector is supposed to follow this slowly moving equilibrium vector very closely. But the reasoning behind why this should work is much clearer, both physically and quantitatively, in the partially diagonalized basis.

Figure 12 shows the process in terms of the partially diagonalized states BV. There are three separate torques acting on the BV, as illustrated in Fig. 13. The BV will precess around the net torque vector \mathbf{Q} at the rate of $|\mathbf{Q}|$. We have already discussed $S\Delta$ and β' . The 2θ comes from the rate of change of the Rabi frequency ratio. To see this, consider the case above in which we start with $g_1=0$ and $g_2=g\neq 0$. Then $\theta=0$ and the atomic state basis and partially diagonalized basis coincide. The initial BV starts at $1\hat{\mathbf{e}}=1\hat{\mathbf{e}}_3$, i.e., all atoms in the $|a\rangle=|-\rangle$ state. We change the Rabi frequency ratio with g held constant so that θ changes linearly in time from 0 to $\pi/2$. If there are no other forces acting on the BV ($S\Delta=\beta'=\alpha=0$, i.e., no fields), then the BV will not move with respect to the atomic state basis, while the partially diagonalized basis will rotate clockwise at the rate of 2θ .

Thus, with respect to the partially diagonalized basis, the BV will rotate counterclockwise at the rate of 2θ .

Now it is simple to see under what conditions low-intensity adiabatic passage will work, with a minimum of loss due to spontaneous emission. The condition for highly coherent adiabatic following is

$$\beta' \gg \sqrt{(2\dot{\theta})^2 + (S\Delta)^2 + \alpha^2}. \quad (52)$$

To see how this works in terms of the atomic state basis, it is helpful to think of a processing top (Fig. 11). The initial condition is $\mathbf{R}_0=1\hat{\mathbf{e}}_3$. As the equilibrium vector \mathbf{R}_S rotates clockwise at the rate of 2θ , the BV tries to catch up with it. There are two types of motion that can help it catch up: precession about \mathbf{Q} and decay at the rate of α . Decay due to α is bad because it corresponds to loss via spontaneous decay. Precession due to $S\Delta$ is also undesirable since it takes the system away from the $|-\rangle$ state in such a fashion that only a decay due to α can reverse the motion. This is to be contrasted with precession due to β' . In this case, the motion is around the equilibrium state ($|-\rangle$) and not away from it. Therefore, decay due to α is not necessary in order to keep the BV close to the equilibrium. Thus we require $\beta' \gg |S\Delta|$. In addition, we require that the precession due to β' be fast compared to the motion of the equilibrium vector about the 2θ torque, that is, $\beta' \gg |2\dot{\theta}|$. This means that a complete half rotation of the BV [i.e., from $\mathbf{R}(t)$ to $\mathbf{R}(t+dt)$] about the equilibrium vector takes place in a very small time, in which the equilibrium vector has moved only slightly [i.e., from $\mathbf{R}_S(t)$ to $\mathbf{R}_S(t+dt)$]. Thus the BV is led to stay around the new equilibrium position. To make sure that very little coherence loss occurs from decay due to α , we further require that $\beta' \gg \alpha$. Figure 12 illustrates the motion of the BV under these conditions.

V. CONCLUSION

One can see the distinct advantages of this Bloch vector model, which holds in the adiabatic following limit. It gives a simple physical picture of the motion. It gives the transient behavior of the system, which in many cases allows one to solve problems by mere inspection. Furthermore, it is independent of the Rabi frequency ratio, handling all cases with equal ease. However, its most important value is in giving the user a quick way to test out particular cases with simple drawings, leading to alternative ideas for applications of the resonant Raman interaction.

ACKNOWLEDGMENTS

We thank Professor Shaoul Ezekiel of MIT for his invaluable contributions. This work was supported by Rome Laboratory Contract No. F 19628-92-K-0013 and Office of Naval Research Grant No. ONR-N0014-91-J-1808.

[1] J. E. Thomas, P. R. Hemmer, S. Ezekiel, C. C. Leiby, Jr., R. H. Picard, and C. R. Willis, Phys. Rev. Lett. **48**, 867 (1982).
 [2] P. R. Hemmer, G. P. Ontai, and S. Ezekiel, J. Opt. Soc. Am. B **3**, 220 (1986).
 [3] P. R. Hemmer, M. S. Shahriar, V. D. Natoli, and S. Ezekiel, J. Opt. Soc. Am. B **6**, 1519 (1989).
 [4] P. Kumar and J. H. Shapiro, Opt. Lett. **10**, 226 (1985).

[5] R. P. Hackel and S. Ezekiel, Phys. Rev. Lett. **42**, 1736 (1979).
 [6] J. Donoghue, M. Cronin-Golomb, J. S. Kane, and P. R. Hemmer, Opt. Lett. **16**, 1313 (1991).
 [7] P. R. Hemmer, D. P. Katz, J. Donoghue, M. Cronin-Golomb, M. S. Shahriar, and P. Kumar, Opt. Lett. **20**, 982 (1995).
 [8] M. S. Shahriar and P. R. Hemmer, in *Coherence and Quantum Optics VII*, edited by J. Eberly, L. Mandel, and E. Wolf (Plenum, 1991), p. 101.

- num Press, New York, 1995), p. 479.
- [9] E. E. Fill, M. O. Scully, and S.-Y. Zhu, *Opt. Commun.* **77**, 36 (1990).
- [10] M. S. Shahriar and P. R. Hemmer, *Phys. Rev. Lett.* **65**, 1865 (1990).
- [11] P. R. Hemmer, M. S. Shahriar, K. Z. Cheng, J. Kierstead, and M. K. Kim, *Opt. Lett.* **19**, 296 (1994).
- [12] J. Gardner, M. L. Marable, G. R. Welch, and J. E. Thomas, *Phys. Rev. Lett.* **70**, 3404 (1993).
- [13] J. Lawall and M. G. Prentiss, *Phys. Rev. Lett.* **72**, 993 (1994).
- [14] L. Goldner, C. Gerz, R. Spreew, S. Rolston, C. Westbrook, W. Phillips, P. Marte, and P. Zoller, *Phys. Rev. Lett.* **72**, 997 (1994).
- [15] M. Kasevich and S. Chu, *Phys. Rev. Lett.* **67**, 181 (1991).
- [16] P. R. Hemmer, M. S. Shahriar, M. G. Prentiss, D. P. Katz, K. Berggren, J. Mervis, and N. P. Bigelow, *Phys. Rev. Lett.* **68**, 3148 (1992).
- [17] P. Marte, R. Dum, R. Taïeb, P. Zoller, M. S. Shahriar, and M. G. Prentiss, *Phys. Rev. A* **49**, 4826 (1994).
- [18] A. Aspect, E. Arimondo, R. Kaiser, N. Vansteenkiste, and C. Cohen-Tannoudji, *Phys. Rev. Lett.* **61**, 826 (1988).
- [19] M. S. Shahriar, P. R. Hemmer, M. G. Prentiss, P. Marte, J. Mervis, D. P. Katz, N. P. Bigelow, and T. Cai, *Phys. Rev. A* **48**, R4035 (1993).
- [20] P. M. Radmore and P. L. Knight, *J. Phys. B* **15**, 3405 (1982).
- [21] P. R. Hemmer and M. G. Prentiss, *J. Opt. Soc. Am. B* **5**, 1613 (1988).
- [22] P. R. Hemmer, M. G. Prentiss, M. S. Shahriar, and N. P. Bigelow, *Opt. Commun.* **89**, 335 (1992).
- [23] M. S. Shahriar, Ph.D. thesis, Massachusetts Institute of Technology, 1992 (unpublished).
- [24] C. Agosta, I. Silvera, H. Stoof, and B. J. Verhaar, *Phys. Rev. Lett.* **62**, 2361 (1989).